Variational Multiscale LES modeling of blood flow in an idealized left human heart

Menghini, F.; Dede', L.; Quarteroni, A.

Variational Multiscale LES modeling of blood flow in an idealized left human heart

Filippo Menghini[a], Luca Dedè[b,*], Alfio Quarteroni[a,b]

[a]*Institute of Mathematics, École Polytechnique Fédérale de Lausanne, Station 8, CH-1015 Lausanne, Switzerland*
[b]*MOX, Dipartimento di Matematica, Politecnico di Milano, Piazza Leonardo da Vinci 32, 20133, Milan, Italy*

Abstract

In this work we build a realistic, although idealized, computational model of the left human heart for the study of the blood flow dynamics. We prescribe the left heart wall displacement based on physiological data and we take into account the presence of both the mitral and aortic valves through a resistive method. We simulate the left heart hemodynamics by means of the Finite Element method and compare different numerical stabilization techniques to account for the transitional and nearly turbulent nature of the blood flow in a physiological regime. In particular, we apply a Variational Multiscale Large Eddy Simulation (LES) model and a Streamwise Upwind Petrov-Galerkin method and we critically analyze the corresponding numerical results.

Keywords: Heart Hemodynamics, Finite Element, Numerical stabilization, VMS-LES, SUPG

1. Introduction

Non-invasive imaging techniques have progressed substantially in recent years and are nowadays widely applied to study the hemodynamics in the heart [1, 2, 3, 4]. In particular, phase-contrast magnetic resonance imaging [5] can be used to visualize and register the heart movements and determine the blood flow velocity. This technique requires to be applied to several heart cycles in order to obtain reliable information on the variables of interest that are indeed averaged over different cycles [1, 2]. Although yielding a meaningful representation of the blood flow in the heartbeat, these techniques cannot provide highly-detailed instantaneous values and cycle-to-cycle variations. Moreover, a more detailed characterization of the blood flow may need some other indicators, such as Wall Shear Stress and Oscillatory Stress Index [6]. Another useful technique is echocardiography, which allows for a better resolution, however at the cost of measuring only one component of the

---

*Corresponding author
Email address:* `luca.dede@polimi.it` (Luca Dedè)

velocity vector, i.e. the one normal to the probe. We refer the reader to [1, 2, 3, 4, 5] for an overview of these techniques applied in both physiological and pathological conditions.

In recent years *in-silico* studies have been increasingly applied to study the hemodynamics in the whole cardiovascular system [7, 8, 9, 10, 11]. Several works focusing on heart valve dynamics, aneurysm and stenosis formation and growth in arteries, fluid-structure interaction between blood and artery walls, and ventricle or heart hemodynamics have been performed with the main focus being the blood flow and its interaction with the surrounding tissue [12, 13, 14, 15, 16, 17, 18, 19, 20, 21, 22, 23]. On the other hand, only few works dealing with the cardiovascular system as a whole and its dynamic response have been performed [7, 24]. Still there is a strong interest in performing patient-specific simulations that could potentially help physicians in assessing the patient condition and eventually leading to personalized therapies. However, this task requires a significantly large amount of computational resources which could be prohibitive if routinely applied in therapy assessment. To overcome this difficulty, reduced order techniques could be exploited by studying parametric models by exploring patient-specific variability to obtain valuable information in a consistent, reliable, and computationally less expensive way [25, 26]. Ahead of this step, one would need to build a representative reference model of the left heart which will stand at the base of further studies of geometric and physical data variability. As inter-patients variability is important to be assessed in this field, the development of a parametrized model could lead to important achievements towards affordable personalized simulation and therapy. Moreover, an idealized geometry which resembles that of a mean adult, can provide a valuable hint on the function of a normal heart.

It has been speculated and reported that the blood flow in the left ventricle is transitional or nearly turbulent [13, 18, 20, 22]. The simulation of a turbulent flow can be based on several approaches. In Direct Numerical Simulations, in principle all the velocity and pressure small scales are numerically solved by using spatial and temporal discretizations which are able to fully resolve Kolmogorov lengths. In Large Eddy Simulations (LES) only the large scales of the solution are directly simulated, whereas the smaller scales are modeled[27, 28]. In this respect, the Variational Multi-Scale (VMS) model represents an alternative way to the widely used Smagorinsky or Germano models in defining a sub-grid model for the LES [29]. As VMS is in fact a stabilization technique for the Navier-Stokes equations, in this work we use both a classical Streamwise Upwind Petrov-Galerkin stabilization method and a VMS-LES model and compare the obtained results to assess their performances and the outputs of interest. We take into account the presence of the heart valves in the human left heart by means of a resistive method, which is embodied in the VMS-LES model [12]. Then, we provide an extensive assessment of the properties of the blood flow in the human left heart by means of an idealized computational model.

This work is organized as follows. We first describe a numerical model for the simulation of an idealized left heart by considering the presence of the heart valves, the prescribed wall displacement and we propose the VMS approach for its numerical simulation. We use physiological data to set up our problem and obtain realistic results. In Section 3 we report the numerical results and compare a few medical outputs with measurements available from literature. Finally, we draw our conclusions.

2

2. Numerical Model

Several aspects need to be taken into consideration for a realistic simulation of the fluid dynamics in the left heart. First, the blood is composed of a liquid phase, the plasma, and of solid cells and platelets carried by the flow, therefore its rheology is rather complex [8, 22, 30]. However, in large vessels as well as in the heart chambers, it can be assumed that the blood behaves like a Newtonian fluid with a constant viscosity. For these reasons, in the following, we assume the blood to be an incompressible Newtonian fluid with constant density $\rho = 1.06$ g/cm^3 and dynamic viscosity $\mu = 0.035$ g/(cm s). These properties are typical of a very viscous fluid, therefore, in small arteries and veins, the flow regime is usually laminar. On the other hand, in the left heart chambers we find the largest velocities, particularly across the valve sections, where the Reynolds number can become as high as 5000 [22]. In these conditions, the flow can become transitional or nearly turbulent and a reliable turbulence model should be considered. The left heart can be considered as a pump that collects the blood from the lungs and pushes it in the aorta, by deforming its shape. The ventricle change in volume is of the order of 70% with respect to its maximum volume while the atrium one is around 30%. To account for these large variations in the geometry, we use an Arbitrary Lagrangian Eulerian (ALE) reference frame. Another important issue is the way valves are accounted for. An approach consists in using a fluid-structure interaction (FSI) model in an ALE framework [13, 15]. The valves are considered as three-dimensional structures and the interface is represented by their lateral surface. Another approach makes use of immersed methods by keeping a single computational domain (the fluid one) and modeling the presence of the valves by means of a resistive method [12, 38]. Other methods consist in mimicking the valves through surrogate models [9] or as time-varying boundary conditions [19].

In this section we discuss all of these issues and how they can be addressed in a unified framework. First, we consider the problem of turbulence modeling and the ALE reference system, then we report the model of the left heart that accounts for the presence of valves, and finally we discuss the boundary conditions for the Navier-Stokes equations.

2.1. Navier-Stokes equations in ALE framework

The Navier-Stokes equations in a moving domain Ω_t that depends on the time t can be written as:

$$\nabla \cdot \mathbf{v} = 0 \qquad \text{in } \Omega_t, \quad t > 0, \tag{1}$$

$$\rho \frac{\hat{\partial} \mathbf{v}}{\partial t} + \rho \left(\mathbf{v} - \mathbf{w}_{ALE} \right) \cdot \nabla \mathbf{v} = \nabla \cdot \mathbf{T}(\mathbf{v}, p) \qquad \text{in } \Omega_t, \quad t > 0, \tag{2}$$

endowed with suitable boundary and initial conditions. In (1-2) ρ is the fluid density, $\frac{\hat{\partial}}{\partial t}$ represents the time derivative in the ALE framework, $\mathbf{w}_{ALE}$ is the domain velocity and the stress tensor $\mathbf{T}(\mathbf{v}, p)$ can be written as a function of the pressure p and of the strain rate

tensor $\mathbf{S}(\mathbf{v})$ as:

$$\mathbf{S}(\mathbf{v}) = \frac{1}{2}\left(\nabla\mathbf{v} + \nabla\mathbf{v}^T\right), \tag{3}$$

$$\mathbf{T}(\mathbf{v}, p) = -p\mathbf{I} + 2\,\mu\,\mathbf{S}(\mathbf{v}), \tag{4}$$

where μ is the dynamic viscosity and p the fluid pressure. We also define the advective velocity $\mathbf{v}_a = \mathbf{v} - \mathbf{w}_{ALE}$. The domain velocity $\mathbf{w}_{ALE}$ is determined by prescribing, for each $t > 0$, its value on the boundary which is then extended in the computational domain through a harmonic extension as [31]:

$$-\nabla \cdot (\mathbf{K}\,\nabla\mathbf{w}_{ALE}) = \mathbf{0} \qquad \text{in } \Omega_t\,, \tag{5}$$
$$\mathbf{w}_{ALE} = \mathbf{w}_{dALE} \qquad \text{on } \Gamma_t\,,$$

where $\mathbf{K}$ is a tensor to be properly set to ensure preservation of the geometric properties of the domain, and later the mesh upon the introduction of the Finite Element discretization, [31].

Now, we introduce the VMS-LES model that is based on the weak formulation of the Navier-Stokes equations. We introduce the infinite dimensional functional spaces needed to write the variational or weak form of (1-2). Let Ω_t be the moving fluid domain and Γ_t its boundary that can be split in $\Gamma_{d,t}$ where a Dirichlet condition is applied and $\Gamma_{n,t}$ where a homogeneous Neumann condition is applied, $\Gamma_t = \Gamma_{d,t} \cup \Gamma_{n,t}$. Then, we define the space of integrable functions in Ω_t as $Q = L^2(\Omega_t)$ and the spaces of weakly differentiable functions $\mathcal{V}_{d,t} = \{\mathbf{u} \in H^1(\Omega_t) : \mathbf{u} = \mathbf{d} \text{ on } \Gamma_{d,t}\}$, where $\mathbf{d}$ is the Dirichlet data on the boundary, and $\mathcal{V}_{0,t} = \{\mathbf{u} \in H^1(\Omega_t) : \mathbf{u} = \mathbf{0} \text{ on } \Gamma_{d,t}\}$. The weak formulation of Navier-Stokes equations in ALE framework is to find, for any $t > 0$, $(\mathbf{v}, p) \in \mathcal{V}_{d,t} \times Q$ such that for all $(\mathbf{w}, q) \in \mathcal{V}_{0,t} \times Q$:

$$\int_{\Omega_t} \nabla \cdot \mathbf{v}\, q\, d\Omega = 0\,, \tag{6}$$

$$\int_{\Omega_t} \left[\left(\rho\frac{\hat{\partial}\mathbf{v}}{\partial t} + \rho(\mathbf{v} - \mathbf{w}_{ALE}) \cdot \nabla\mathbf{v}\right) \cdot \mathbf{w} + \mathbf{T}(\mathbf{v}, p) : \nabla\mathbf{w}\right] d\Omega = 0\,. \tag{7}$$

We now assume a multiscale decomposition of each of the spaces $\mathcal{V}_{d,t}$, $\mathcal{V}_{0,t}$ and Q in the form $S = S^h \oplus S'$ with S^h a suitable finite dimensional space and S' an infinite dimensional one. The space S^h is built by means of the finite element space $\mathcal{X}_h^r = \{\mathbf{v}_h : \Omega_t \to \mathcal{R} : \mathbf{v}_h|_k \in \mathcal{P}_r \quad \forall k \in \tau_h\}$, with r the polynomial degree and τ_h the partition of Ω_0 into mesh elements (tetrahedrons in our case); the rest of the space notation is understood. In this way, every function we have defined on the spaces $\mathcal{V}_{d,t}$, $\mathcal{V}_{0,t}$ and Q, can be written as the sum of a coarse scale and a fine scale component,

$$\mathbf{v} = \mathbf{v}^h + \mathbf{v}' \qquad p = p^h + p' \qquad \mathbf{w} = \mathbf{w}^h + \mathbf{w}' \qquad q = q^h + q'\,.$$

By representing (6-7) into coarse and fine scale components and integrating by parts the fine scale terms into the coarse scale equations we obtain the coarse equations, with the fine

scale terms not appearing under differential operators [29, 32]. We can close the problem by modeling the fine scales as:

$$\mathbf{v}' = -\tau_M(\mathbf{v}^h)\,\mathbf{r}_m(\mathbf{v}^h, p^h) \tag{8}$$

$$p' = -\tau_C(\mathbf{v}^h)\,r_c(\mathbf{v}^h)\,, \tag{9}$$

where $\mathbf{r}_m(\mathbf{v}^h, p^h)$ and $r_c(\mathbf{v}^h)$ are the element-wise strong residuals of (2) and (1), respectively:

$$\mathbf{r}_m(\mathbf{v}^h, p^h) = \rho\frac{\hat{\partial}\mathbf{v}^h}{\partial t} + \rho(\mathbf{v}^h - \mathbf{w}_{ALE})\cdot\nabla\mathbf{v}^h - \nabla\cdot\mathbf{T}(\mathbf{v}^h, p^h)\,, \tag{10}$$

$$r_c(\mathbf{v}^h) = \nabla\cdot\mathbf{v}^h\,. \tag{11}$$

The stabilization parameters $\tau_M(\mathbf{v}^h)$ and $\tau_C(\mathbf{v}^h)$ will be defined later. In this work we use a Backward Differentiation Formula (BDF) of order σ to advance the ordinary differential problem in time, once the Finite Element space discretization of the equations has been achieved. In order to address the nonlinear nature of these equations it is necessary to solve a nonlinear problem, by means of, e.g., Picard fixed point or Newton iterations. It is also possible to use a semi-implicit formulation [32]. Here the nonlinear terms are linearized by means of a Newton-Gregory extrapolation of order σ of the variables in the nonlinear terms. The extrapolation is based on the solution at the previous time steps [32]. In this way the equations are linear and can be solved once at each time step. This method is computationally cheaper than Newton method, for instance, but there might be a restriction on the time-step to be used in the BDF discretization to obtain reliable and stable results.

2.2. Left heart geometry and wall displacement

The left heart (LH) is composed of two chambers, the left atrium (LA) and the left ventricle (LV), which are separated by the mitral valve. Four pulmonary veins (PV) are connected to the left atrium (LA) and the aorta is connected to the LV through the aortic valve (AV). The LH geometry consists of an idealized LA (see [33, 34]) anchored to an idealized LV represented by half of a prolate ellipsoid, see [18, 19, 20]. In this work, we match the base of the LA with the LV through an idealized mitral valve section which is about 5 cm^2 large. Moreover, we model the aortic root as a cylinder whose diameter is $D_{AV} = 3$ cm and the pulmonary veins as four equally sized cylinders with diameter $D_{PV} = 1.5$ cm. The geometry of the idealized LH at the end systolic phase, i.e. when the LV volume is smaller than the LA one, is reported in Figure 1. Here we consider only the volume occupied by the blood, so that there are time intervals of the heartbeat during which the LV volume is actually smaller than the LA one. In the time instant reported in Figure 1, corresponding to $t = 0$ s in Figure 3, the LV volume is approximately 53 mL, while the LA one is 92 mL. The left atrial appendage (LAA) is a small chamber linked to the atrium through an orifice. Its morphology is variable among individuals and four reference types have been classified [35]. The one reported in Figure 1 approximately corresponds to a "CauliFlower" type LAA; see [21, 35].
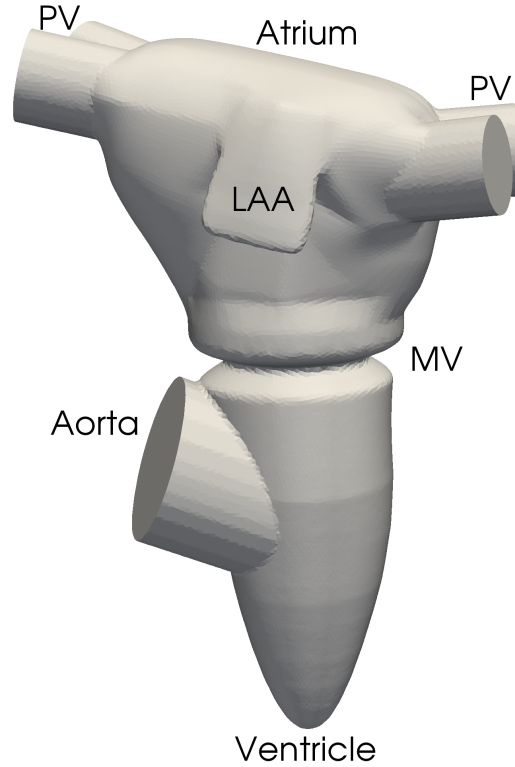
5

Figure 1: The idealized LH geometry at the end systolic phase. The atrium (LA) is located over the ventricle (LV) and the two chambers are separated by the mitral valve section (MV), the pulmonary veins (PV) and the left atrial appendage (LAA) are also indicated. The aortic root is attached to the LV.

The physiological heart cycle is divided into two main phases, the diastole and the systole. We define T_{hb} the total time length of one heartbeat, t_{dias} the time length of the diastole and t_{syst} the systole one. During diastole, blood enters in the LA from the pulmonary veins and flows to the LV passing through the MV, which is open. The AV is closed so that the blood cannot flow out of the LV. The LV expands during this phase while the LA reduces its size. The volume reduction of the LA is due to the LV movement towards the LA and to an atrial contraction during the last part of the diastole. When the LV stops expanding and starts contracting, the MV closes due to the pressure difference; a very fast iso-volumetric phase takes place in which the LV pressure rises until it overtakes the aortic pressure, so that the AV opens. The systole is the phase during which the LV contracts, the oxygenated blood is pushed from the LV into the aorta, the LA dilates and is filled with blood coming from the PVs. In this phase, the MV is closed. Finally, after the LV has attained its minimum volume, it starts expanding again, the intraventricular pressure drops and the AV closes due to the pressure difference between the aorta and the LV. There is another very fast iso-volumetric phase in which both of the valves are closed and the LV pressure drops until it reaches the LA values, then the MV opens and a new cycle begins. These phases are represented in the well known Wiggers diagram
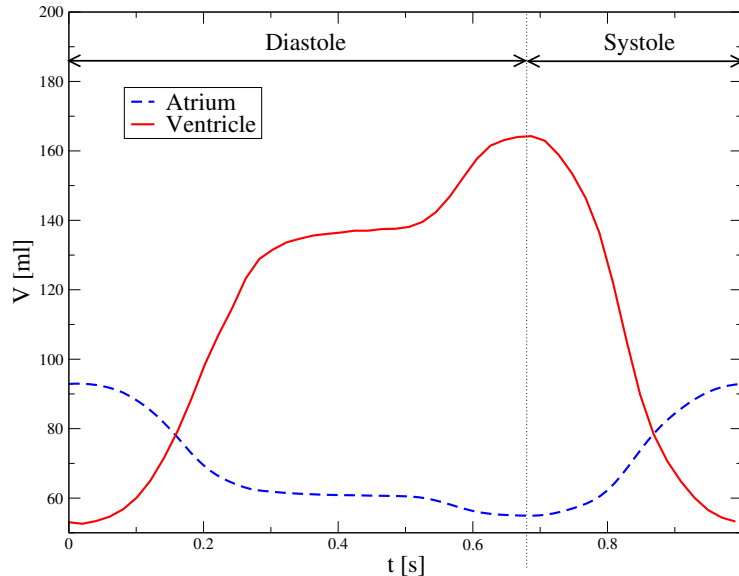
6

Figure 2: Volumes of the atrium and ventricle as a function of time.

[8, 36]. From a modeling point of view, since we assume the blood to be an incompressible fluid, we cannot straightforwardly represent the iso-volumetric phases when the pressure change is due to small volume variations. With this aim, one should allow some limited compressibility to the fluid so that this process can be captured. However, since these phases are fast, we assume the switch between diastole and systole is instantaneous as well as the valves change in configuration from open to closed. Therefore, there are only two possible configurations in our model: diastole with expanding LV, contracting LA, MV open and AV closed and systole with contracting LV, expanding LA, MV closed and AV open.

To model the wall displacement of the LH, we assume the variations in volume to be in the physiological range, with the LV volume in the range of 53 to 164 mL while LA spans between 55 to 92 mL [3]. To define the wall movement, we assume several other constraints: the ratio between the height and the diameter of the LV is kept around $1.7 \div 2$ [18, 22, 37]. Moreover, the LV apex movement is directed towards the LA, as it is known from medical images. Finally, we assume that the LA volume variation is similar to the one of a sphere with changing volume, so that the displacement is directed towards the center of the LA. With these constraints, we proceed by decomposing the wall dependence in time and in space. The volume variation in time should correctly represent two different filling stages of the LV during diastole, called the Early wave (E-wave) and the After wave (A-wave). We report in Figure 2 the volume versus time for the idealized LV and LA. These are obtained with a Fourier expansion in time of the volume function in [18] that has been also adapted to the LA problem. In Figure 3 we display snapshots of the geometry of the LH at several time instants. Being based on an analytical characterization of the wall displacement, our model can be easily parametrized in order to represent a wide range of physiological variability among patients.
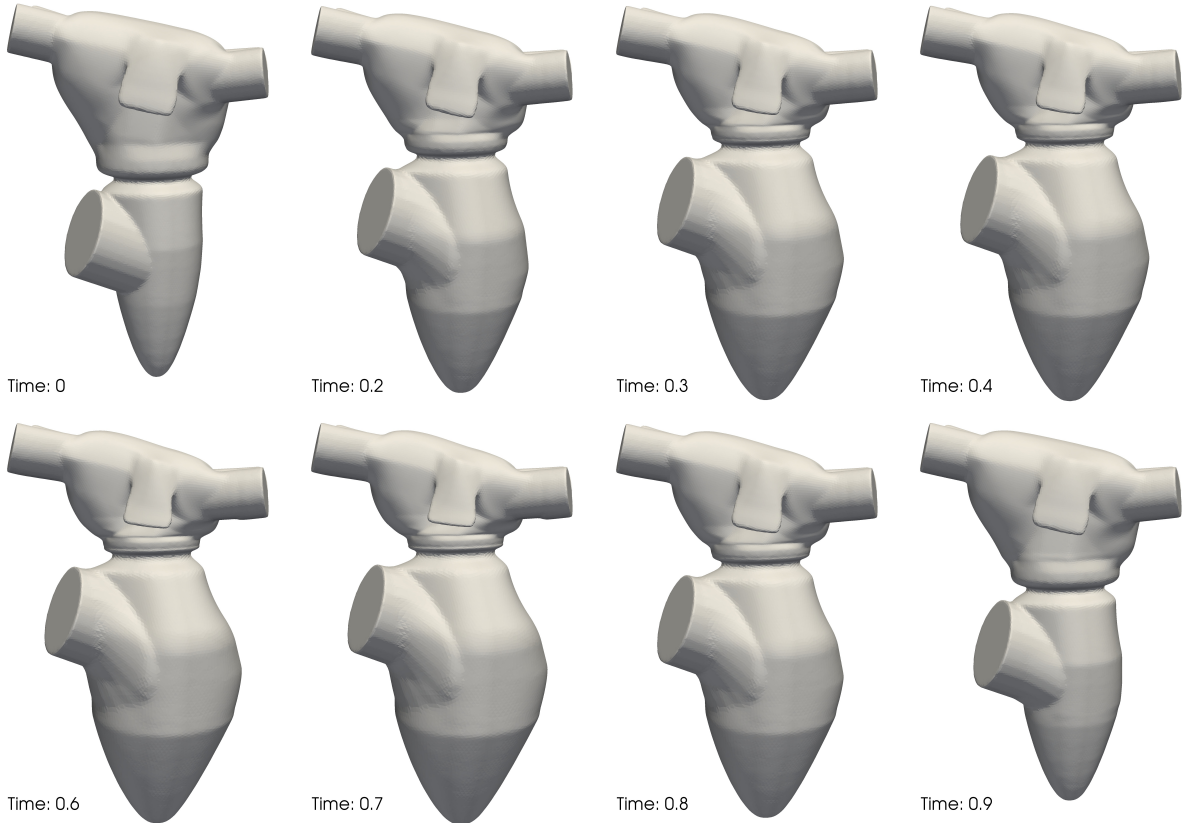
7

Figure 3: Snapshots of the LH geometry at different time instants of the heartbeat.

2.3. Heart valves

Modeling the heart valves is a problem that has and is currently being extensively studied, see e.g. [12, 13, 15, 16, 17, 24, 38]. The dynamics of the leaflets is very complex and subject to strong fluid-structure interaction. In some preliminary studies [24], the valve dynamics is approximated by a zero-dimensional model, according to which the state of the valve is completely determined by a few variables, such as the leaflets angle or the valve open area. Usually, these models take into account the pressures at both sides of the valve, the blood flux through the valve and few other variables, yielding a system of Ordinary Differential Equations (ODEs) [12, 24]. In other works [13, 16, 17, 38], the valve is instead considered as a three-dimensional object and a full fluid-structure interaction problem should be solved, either in a moving mesh framework or with immersed methods. In this work, we assume that the valve dynamics is known *a priori* and that the interactions of the valve with the fluid are limited to a no-slip condition at the valve leaflets or, better said, that the fluid adheres to the valve. That is, similarly to [19, 20], we model only the fluid problem in a deforming domain. To achieve this goal we use a resistive method as in [12], and we assume the valves to be in either their open or closed configurations. We do not explicitly represent the valve leaflets, but rather we let them "disappear" in the valve open configuration. Then, we identify the regions (AV for aortic valve and MV for mitral
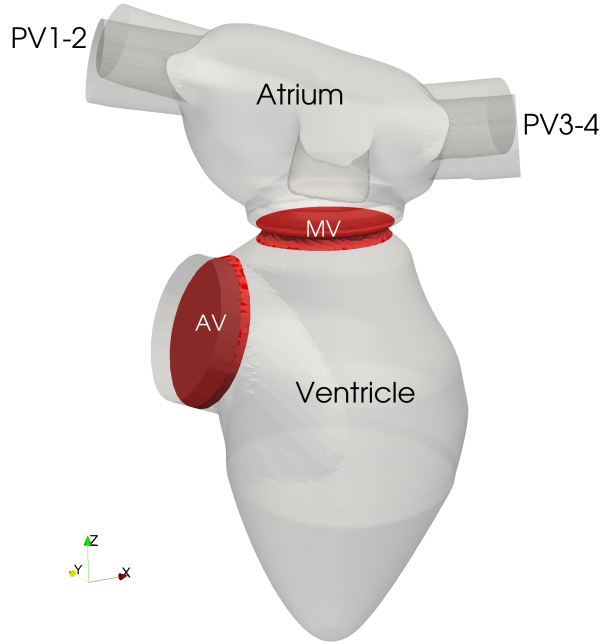
8

Figure 4: Locations of the mitral and aortic valves. The subsets of the geometry in red stands for the region in the domain where the velocity is enforced to adhere to the domain velocity when the valves are closed, i.e. during diastole for the aortic valve and during systole for the mitral valve.

valve) occupied by the valves in their closed configurations in which we set the velocity to be equal to the domain velocity $\mathbf{w}_{ALE}$. In Figure 4, we report the location where we enforce the fluid velocity to be equal to the domain velocity. We remark that the aortic valve is closed during diastole, while the mitral valve is closed during systole.

To account for the valves with the resistive method, the momentum equation in the Navier-Stokes equations (6-7) is supplemented with an additional term,

$$\int_{\Omega_t} R_h \left(\mathbf{v} - \mathbf{w}_{ALE}\right) d\Omega \,, \tag{12}$$

where the function R_h has support in the subsets of Ω_t where the valves lay; $\|R_h\|_L^2(\Omega_t)$ is "sufficiently" large to effectively enforce the adherence of the fluid velocity to the domain motion velocity $\mathbf{w}_{ALE}$. Note that $R_h = R_h(\mathbf{x}, t)$ [12]. In this work, after Finite Element discretization in space, we use a function R_h which is piecewise discontinuous onto the Finite Element mesh.

The standard VMS-LES formulation of the Navier-Stokes equations is modified to account for the presence of the resistive term. The definition of the stabilization parameters

9

is [12, 29, 32]:

$$\tau_M(\mathbf{v}^h) = \left(\frac{\rho^2 \sigma^2}{\Delta t^2} + \rho^2 \, \mathbf{v}_a^h \cdot \mathcal{G} \, \mathbf{v}_a^h + \overline{C} \mu^2 \, \mathcal{G} : \mathcal{G} + R^2 \right)^{-\frac{1}{2}}, \tag{13}$$

$$\tau_C(\mathbf{v}^h) = \frac{1}{\tau_M(\mathbf{v}^h) \mathbf{g} \cdot \mathbf{g}}, \tag{14}$$

where σ is a constant equal to the order of the time discretization based on BDF (Backward Differentiaion Formulas), $\overline{C} = 60$, $\mathcal{G}$ is a second-rank metric tensor and $\mathbf{g}$ is the metric vector:

$$\mathcal{G} = \left(\frac{\partial \xi}{\partial \mathbf{x}} \right)^T \frac{\partial \xi}{\partial \mathbf{x}}, \tag{15}$$

$$\mathbf{g} = \sum_{j=1}^{3} \left(\frac{\partial \xi}{\partial \mathbf{x}} \right)_{ji}, \tag{16}$$

where $\frac{\partial \xi}{\partial \mathbf{x}}$ is the inverse Jacobian of the mapping between the reference and the physical domain. See [29, 32] for more details.

To summarize, the VMS-LES formulation with resistive term is: find, for each time $t > 0$, $(\mathbf{v}^h, p^h) \in \mathcal{V}_{d,t}^h \times Q^h$ such that, for all $(\mathbf{w}^h, q^h) \in \mathcal{V}_{0,t}^h \times Q^h$

$$\int_{\Omega_t} \left(\nabla \cdot \mathbf{v}^h \, q^h - \mathbf{v}' \cdot \nabla q^h \right) d\Omega = 0, \tag{17}$$

$$\int_{\Omega_t} \left[\left(\frac{\hat{\partial} \mathbf{v}^h}{\partial t} + \rho(\mathbf{v}_h - \mathbf{w}_{ALE}) \cdot \nabla \mathbf{v}^h + R \left(\mathbf{v}^h - \mathbf{w}_{ALE} \right) \right) \cdot \mathbf{w}^h + \mathbf{T}^h : \nabla \mathbf{w}^h \right] d\Omega \tag{18}$$

$$- \int_{\Omega_t} \left[\mathbf{v}' \cdot (\rho(\mathbf{v}_h - \mathbf{w}_{ALE}) \cdot \nabla \mathbf{w}^h) - p' \nabla \cdot \mathbf{w}^h \right] d\Omega$$

$$- \int_{\Omega_t} \mathbf{v}' \cdot (\rho(\mathbf{v}_h - \mathbf{w}_{ALE}) \cdot (\nabla \mathbf{w}^h)^T) \, d\Omega$$

$$- \int_{\Omega_t} (\mathbf{v}' \otimes \mathbf{v}') \cdot \nabla \mathbf{w}^h \, d\Omega = 0,$$

together with initial conditions $\mathbf{v} = \mathbf{0}$, $p = 0$ and the fine scale velocity and pressure $\mathbf{v}'$, p' defined as in (8-9). The definition of the residual $\mathbf{r}_m(\mathbf{v}^h, p^h)$ in (8) is modified, to account for (12),

$$\mathbf{r}_m(\mathbf{v}^h, p^h) = \rho \frac{\hat{\partial} \mathbf{v}^h}{\partial t} + \rho(\mathbf{v}^h - \mathbf{w}_{ALE}) \cdot \nabla \mathbf{v}^h + R_h \left(\mathbf{v}^h - \mathbf{w}_{ALE} \right) - \nabla \cdot \mathbf{T}(\mathbf{v}^h, p^h). \tag{19}$$

We remark that in (18) the first integral is the residual of the momentum equation, the second integral accounts for a SUPG stabilization term, the third integral is a stabilization term due to the VMS model and the fourth integral is the Reynolds stress term, which yields the VMS-LES modeling using (8).

10

2.4. Boundary conditions

Based on the Wiggers diagram, the boundary conditions differ when considering diastole and systole since the valve behavior has a strong influence on the flow. In particular, during diastole, the AV is closed and the whole volume variation of the LH must be balanced by an equal blood inflow from the PVs. During systole, the flow rate in the LA coming from the PVs must be equal to the LA volume variation, while the aorta outflow is equal to the LV volume variation. Since the flow is periodic, we define the boundary conditions on a time period corresponding to one heartbeat time T_{hb}, and then, at each new heartbeat, the same boundary conditions are applied. By defining $t^* \in [0, T_{hb})$ as the time in one heartbeat we have

$$
Q_{PV} = \begin{cases} \dfrac{dV_{ven}}{dt} + \dfrac{dV_{atr}}{dt} & t^* \in [0, t_{dias}] \\[3mm] \dfrac{dV_{atr}}{dt} & t^* \in (t_{dias}, T_{hb}) \end{cases} \tag{20}
$$

We assume the inflow at the PVs to be equally split among the veins, and a parabolic velocity profile for the blood in the veins, as this flow can be assumed to be laminar. To define a parabolic profile in each vein, we solve an additional problem for a scalar variable χ in the volume Ω_t, see Figure 1, written as:

$$
\begin{aligned}
-\Delta \chi &= 1 & \text{in} \quad & \Omega_t \,, \\
\chi &= 0 & \text{on} \quad & \Gamma_w \,, \\
\nabla \chi \cdot \mathbf{n} &= 0 & \text{on} \quad & \Gamma_{PV} \,,
\end{aligned} \tag{21}
$$

where $\Gamma_{PV,t}$ is the inlet surface of the pulmonary veins and $\Gamma_w = \partial\Omega_t \backslash \Gamma_{PV,t}$. The variable χ represents the value of the blood velocity normal to the PV sections. With this variable we define a reference inflow velocity profile $\mathbf{v}_{ref}^i$ with total flux equal to 1 on each i inlet vein as

$$
\mathbf{v}_{ref}^i = \frac{\chi \mathbf{n}}{\int_{\Gamma_{PV}^i} \chi d\Gamma} \qquad i = 1, 2, 3 \,,
$$

where $\mathbf{n}$ is the unit vector normal to Γ_{PV}^i and Γ_{PV}^i is the subset of Γ_{PV} to a single pulmonary vein $i = 1, 2, 3$. Given an inflow flux Q_{PV}, we rescale the velocity $\mathbf{v}_{ref}^i$ to obtain the Dirichlet boundary condition at the pulmonary vein simply as $\mathbf{v}|_{\Gamma_{PV}^i} = 0.25\, Q_{PV}\, \mathbf{v}_{ref}^i$. On the last pulmonary vein, $i = 4$, we set a Neumann boundary condition to impose the pressure in the atrium during the whole cycle. Based on physiological data, we choose the pressure at the 4th pulmonary vein to be equal to 10 mmHg.

The boundary conditions at the outlet of the left heart, namely at the aorta section behind the aortic valve, should take into account the rest of the cardiovascular system as well as its resistance to the fluid exiting from the heart. A common way to accommodate this request is to use boundary conditions of resistance type [39, 40, 41]. The stress on the outlet section is split in its normal and tangential components. Then, the tangential

components are set to zero, whereas the normal component is expressed as the sum of two terms, one assigning the minimum pressure of the system and the second one accounting for a resistance due to the outflow. In summary, after denoting the normal vector to the outlet with $\mathbf{n}$ and the tangential vectors with $\mathbf{t}_1$ and $\mathbf{t}_2$, we set

$$\mathbf{T}\,\mathbf{n} = -(C_r Q_{out} + p_{ao})\mathbf{n}\,, \qquad \mathbf{T}\,\mathbf{t}_1 = \mathbf{0}\,, \qquad \mathbf{T}\,\mathbf{t}_2 = \mathbf{0}\,,$$

where Q_{out} is the blood flux through the aortic section, $Q_{out} = \int_{\Gamma_{ao}} \mathbf{v} \cdot \mathbf{n}\, d\Gamma$, C_r is a constant that has to be set up to obtain a correct physiological pressure during systole, and p_{ao} is the minimum pressure in the aorta. During diastole, we assume $C_r = 0$ and we set the aortic pressure as linear in time with physiological values extrapolated from the Wiggers diagram. During systole, the resistance of the circulatory system is active, and we set a minimum arterial pressure of 70 mmHg. Therefore:

$$C_r = \begin{cases} 0 & t^* \in [0, t_{dias}] \\[2mm] 400 & t^* \in (t_{dias}, T_{hb}] \end{cases}$$

$$p_{ao} = \begin{cases} 70\left(1 - 20\dfrac{t^* - t_{dias}}{t_{dias}}\right) & t^* \in [0, t_{dias}] \\[3mm] 70 & t^* \in (t_{dias}, T_{hb}] \end{cases}$$

where the units are [dyn s/cm^5] for C_r and [mmHg] for the pressure.

3. Numerical results and discussion

Our numerical simulations were carried out by means of the computing resources of the Swiss National Supercomputing Center (CSCS) in Lugano using up to 20 nodes of Piz Daint Cray XC40 system. We used P1-P1 tetrahedral linear elements and a Backward Differentiation Formula of order $\sigma = 2$ for the time integration and equal order extrapolation for the nonlinear terms, see [32]. Our software implementation was realized in the open-source finite element library LifeV [42]. We tested both the VMS-LES formulation as reported in (17-18) and a SUPG stabilization. The latter is simply realized by removing the last two terms on the left hand side of Eq. (18). For both stabilization methods, in order to obtain a fully developed flow, we started the computation with a null solution and disregarded the first two heartbeats. Then, the simulation is continued for further four heartbeats.

We tested several meshes progressively refined and we selected the one with $3'343'277$ elements and $2'170'320$ degrees of freedom. This choice was made upon checking *a posteriori* the LES quality of the simulation by using the Pope criterion presented in [27]. According to [27], the fraction of the turbulent kinetic energy in the resolved motions is defined as

$$M_h(\mathbf{x}, t) = \frac{k_r(\mathbf{x}, t)}{K_h(\mathbf{x}, t) + k_r(\mathbf{x}, t)}\,, \tag{22}$$

12

where k_r is the kinetic energy of the unresolved scales and K_h is the kinetic energy of the resolved scales,

$$K_h = \int_{\Omega(t)} \frac{\rho}{2} \mathbf{v}_h(\mathbf{x}, t) \cdot \mathbf{v}_h(\mathbf{x}, t) \, d\Omega, \tag{23}$$

which is available through the computed velocity $\mathbf{v}_h$. Therefore, M_h is a measure of how much energy is actually resolved in the numerical simulation; to perform a "good" quality LES we set a maximum value of $M_h^{max} = 0.2$ [27] everywhere in the computational domain. If the value of M_h is larger than M_h^{max}, then one would need to refine the computational mesh. The problem in this method is how to compute the kinetic energy of the unresolved scales. In our residual based VMS-LES formulation we propose to use (8) to approximate the unresolved scales and to compute M_h as follows

$$M_h(\mathbf{x}, t) = \frac{\int_{\Omega(t)} \mathbf{v}' \cdot \mathbf{v}' \, d\Omega}{\int_{\Omega(t)} \mathbf{v}_h \cdot \mathbf{v}_h \, d\Omega + \int_{\Omega(t)} \mathbf{v}' \cdot \mathbf{v}' \, d\Omega}. \tag{24}$$

We checked the results of the simulations and we found that with this mesh the largest values of M_h are observed close to the valves and the LA and LV walls, but these never exceed the value M_h^{max}. Far from the walls and the valves, we have $M_h < 10^{-4}$ so we assume that the flow is well resolved with this mesh.

We now describe the flow results obtained with the VMS-LES stabilization method and a time step of $\Delta t = 4 \cdot 10^{-4}$ s. The flow in the left heart features a very complex pattern; to visualize it, we use the volume rendering of the velocity magnitude in Figure 5 and, in Figure 6, the Q-criterion. The latter represents a standard way to visualize coherent vortex structures in the flow [34]. The Q function is

$$Q = 0.5(|\mathbf{A}|_2 - |\mathbf{S}|_2),$$

where $\mathbf{A}$ and $\mathbf{S}$ are, respectively, the antisymmetric and symmetric part of the velocity gradient. Coherent vortex structures appear in regions of a positive Q; in order to visualize them, we plot the iso-contours of Q by selecting a suitable positive value.

In Figure 5, we report the velocity magnitude in the left heart at several instants of the sixth heartbeat, when the flow is fully developed. In Figure 6, we display the iso-contours of $Q = 500$ colored according to the velocity magnitude, in the same heartbeat. During early diastole, the velocity is very small, especially in the LV, with some structures still visible in the LA. When the E-wave starts, a high speed flux crosses the MV section and produces a large non-symmetrical structure in the upper part of the LV. The jets coming from the PVs impact in the center of the LA and then progressively dissipate until the A-wave starts. The blood flux through the MV generates a coherent structure in the LV, the so-called O-ring [18, 22, 43]. The latter breaks into smaller structures as the blood flow moves towards the apex and finally impinges the LV wall. Within the A-wave, a small vortex structure is visible under the mitral section but it is broken immediately at the MV closure and the opening of the AV which marks the beginning of the systole. During systole, a high velocity jet is visible in the aorta and the coherent structures present in the
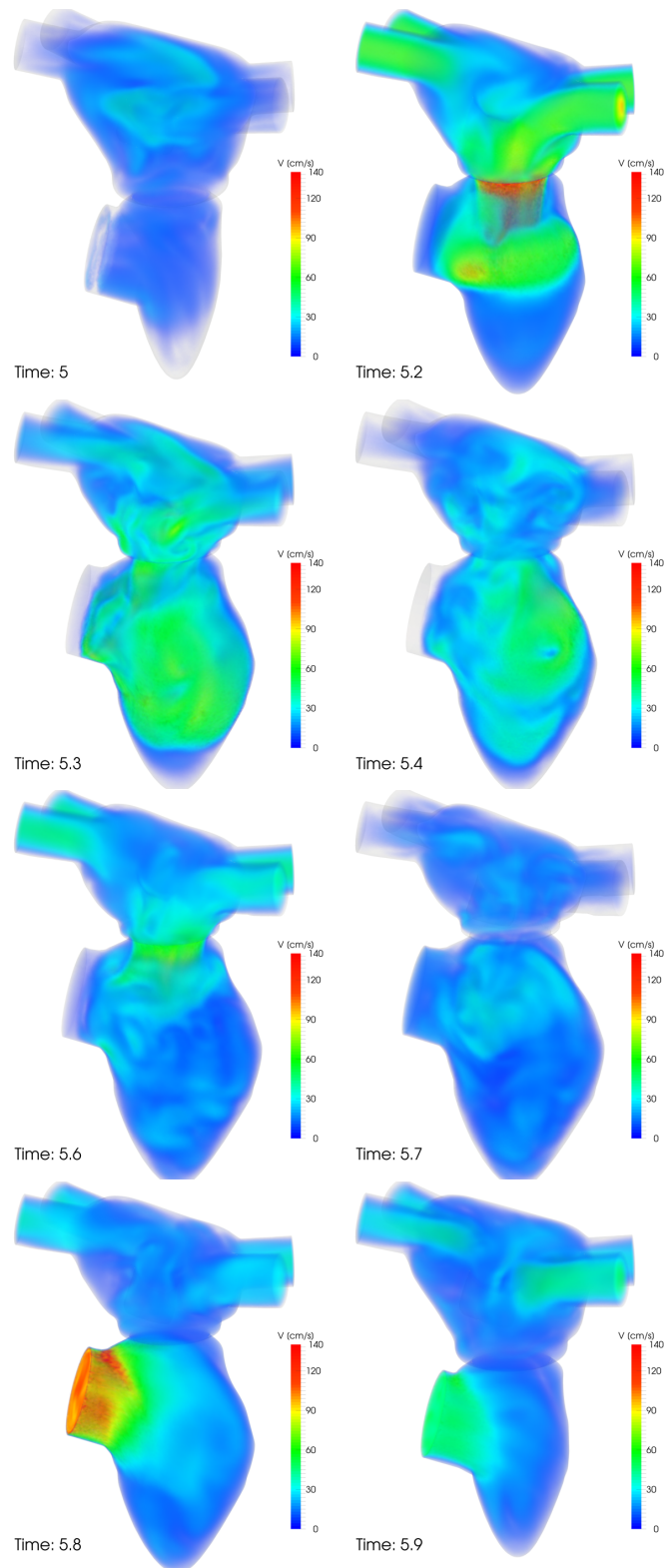
Figure 5: Snapshots of velocity magnitude (volume rendering) at different time instants of the heartbeat.
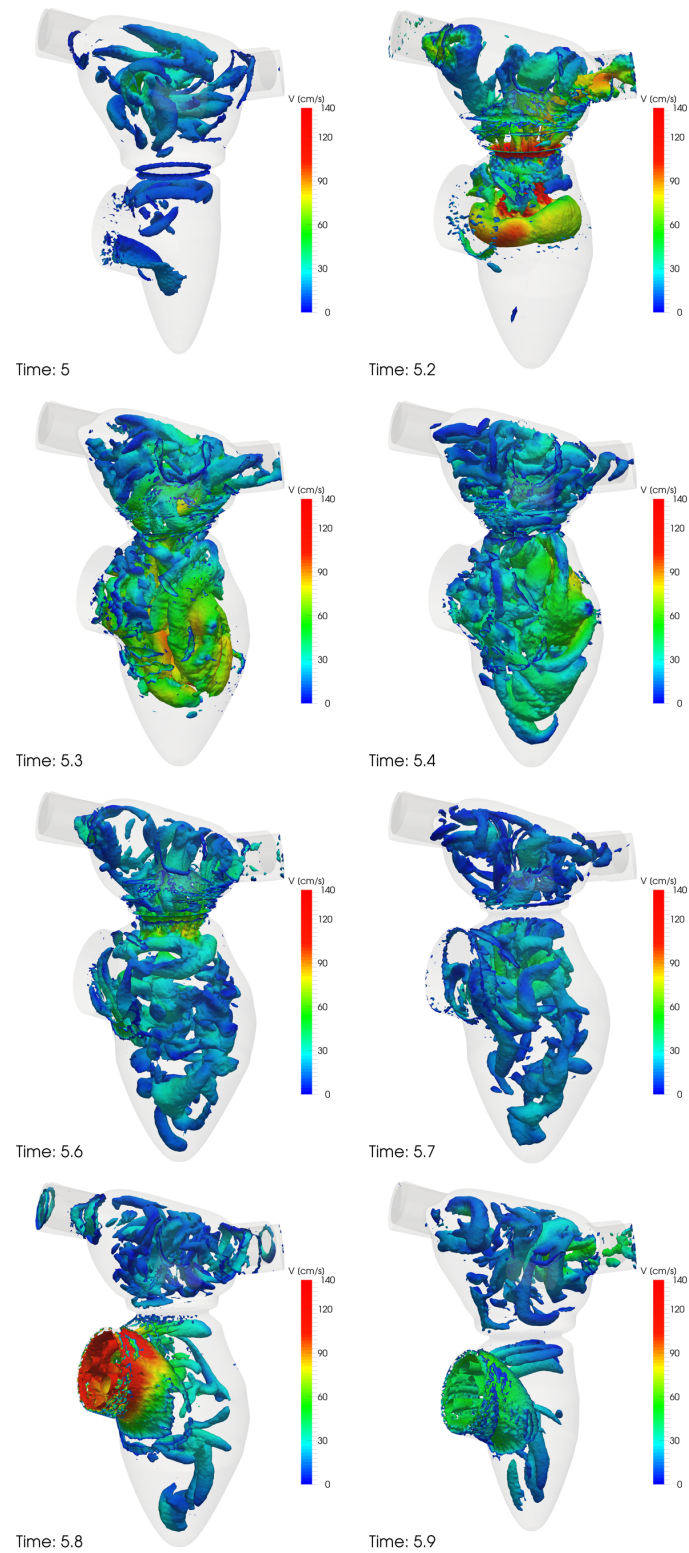
Figure 6: Snapshots of Q-criterion contours (for $Q = 500$) colored by the velocity magnitude at different time instants of the heartbeat.
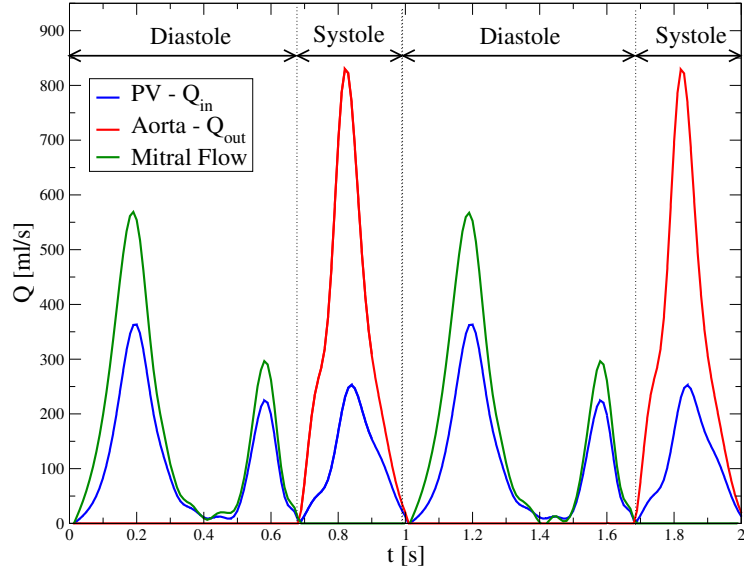
15

Figure 7: Flow rates through the PVs, the MV section and the aortic section versus time along two heartbeats.
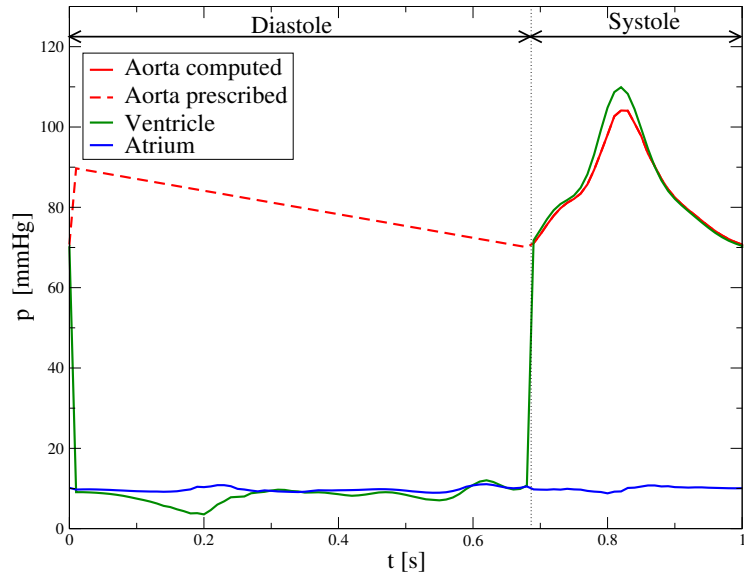

Figure 8: Average pressure in the LA, LV and aorta versus time along one heartbeat.

LV are flushed out with the blood flow. The LA is refilled with blood coming from the PVs that produces again an impact between jets, although weaker than the one of the E-wave. At the end of the systole, some structures are still visible in the LA and a small one in the LV just under the mitral section. The velocity is very small apart from the aorta and the veins where inertia is still mixing the blood. All of these features of the blood flow are consistent with those reported in [18, 19, 20, 22, 43].

We post-process the results to obtain the flow rates at the inlet, outlet and mitral
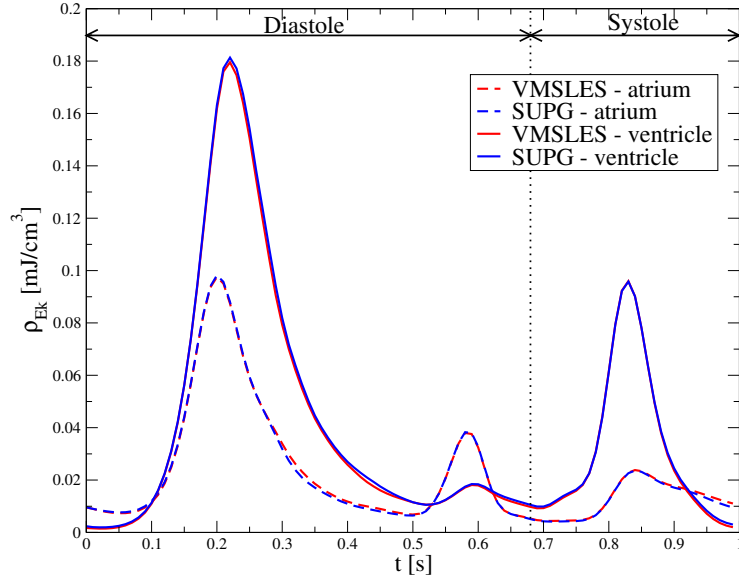
16

Figure 9: Specific kinetic energy ρ_{Ek} in the LV and in the LA of the idealized LH versus time in a phase averaged heartbeat. Results obtained with VMS-LES and SUPG stabilization.

sections as reported in Figure 7. The inlet and outlet blood flow rates versus time are reported for the first two heartbeats but, since they correspond to the volume variations, these show negligible differences among cycles. The mitral flow, on the other hand, could vary since it depends on the blood flow that develops in the LH; however, we notice that this variable shows the same behavior in time among different heartbeats. A possible explanation is that the mitral flow depends mostly on the wall displacement and volume variations and not on specific features of the flow and geometry. In Figure 8, we report the average pressure computed in the LA, in the LV and on the aorta section versus time, for one heartbeat. To evaluate the average pressure in the LA and in the LV, we selected a small volume in approximately the center of each of these chambers and averaged therein the value to obtain the data plotted in Figure 8. In a similar way, we selected a small area in the center of the aorta section and averaged to obtain the pressure at the aorta section. We remark that the pressure in the aorta is prescribed during diastole and that during the first cycle we increase its value starting from zero. During systole, the pressure in the aorta is obtained using the resistance outlet boundary condition [19, 39, 40, 41]. The pressure in the LA shows small oscillations around the average value of 10 mmHg that can be linked to the blood flow coming from the veins. On the other hand, the pressure in the LV increases when the MV closes and overcomes the pressure in the aorta. In late systole the aortic pressure overcomes the LV pressure and this leads to the closing of the aortic valve with a delay, if a proper valve model is used. In our model the aortic valve simply closes at a fixed time and the LV pressure falls down again to values similar to the LA ones because of the MV opening. The plots of the flow rates and pressure obtained show the same features of the Wiggers diagram.

The blood flow is periodic; in order to study a representative blood flow among different
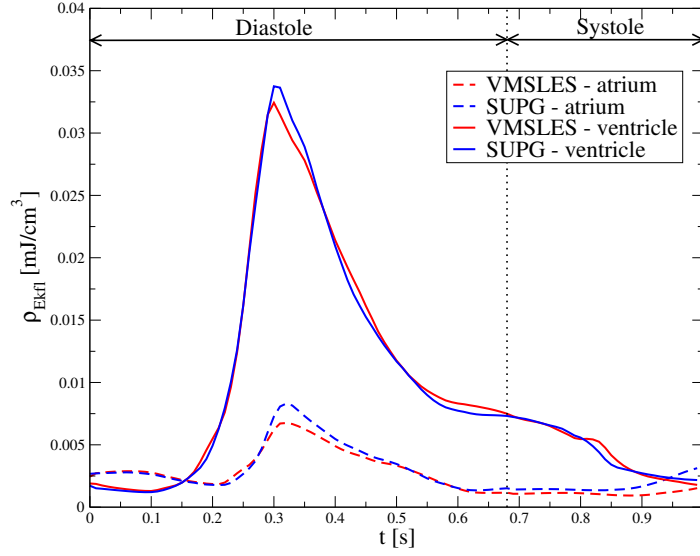
17

Figure 10: Specific fluctuating kinetic energy ρ_{Ekfl} in the LV and in the LA of the idealized LH versus time in a phase averaged heartbeat. Results obtained with VMS-LES and SUPG stabilization.

Figure 11: Specific enstrophy ρ_S in the LV and in the LA of the idealized LH versus time in a phase averaged heartbeat. Results obtained with VMS-LES and SUPG stabilization.
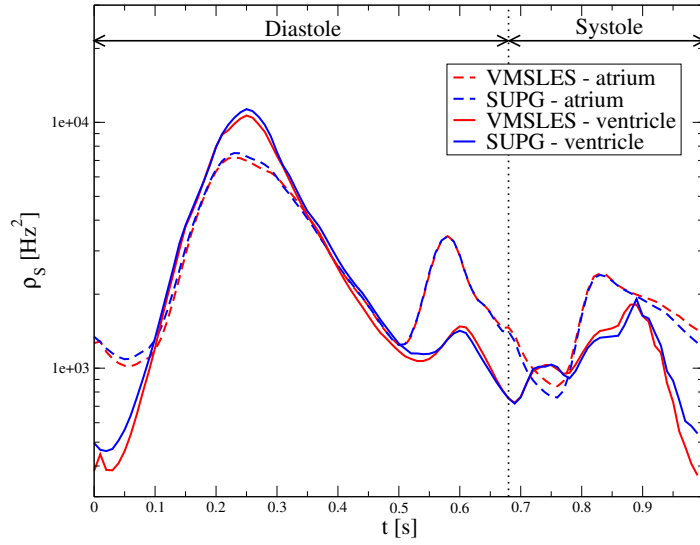
heartbeats, we perform a phase averaging of the variables defining the phase average of the

	Diastole	Systole
LV VMS-LES	5.06 mJ	3.35 mJ
LA VMS-LES	1.80 mJ	0.95 mJ
LV SUPG	5.19 mJ	3.40 mJ
LA SUPG	1.79 mJ	0.94 mJ
Healthy LV [2]	2.0 ± 0.8 mJ	1.6 ± 0.6 mJ
Diseased LV [2]	3.2 ± 2.3 mJ	2.2 ± 1.4 mJ

Table 1: Average kinetic energy in the LV and LA obtained with VMS-LES turbulence model, SUPG stabilization and measured experimentally [2].

velocity and its root mean square as:

$$\overline{v}_i(\mathbf{x}, t^*) = \frac{1}{N_c} \sum_{j=0}^{N_c-1} v_i(\mathbf{x}, t^* + j\, T_{hb}) \qquad t^* \in [0, T_{hb}], \qquad i = 1, 2, 3\,, \tag{25}$$

$$v_i^{rms}(\mathbf{x}, t^*) = \frac{1}{N_c} \sum_{j=0}^{N_c-1} \sqrt{\overline{v_i^2}(\mathbf{x}, t^* + j\, T_{hb}) - \overline{v}_i^2(\mathbf{x}, t^*)} \qquad t^* \in [0, T_{hb}], \quad i = 1, 2, 3\,. \tag{26}$$

We set $N_c = 4$ and we discard the first two heartbeats to remove the influence of the non-physical initial condition. The quantity $\mathbf{v}^{rms}$ provides information on the flow variability among heartbeats and can be used as an indicator of transition to turbulence [20]. With these phase averaged quantities we compute some global indicators of the flow, such as the total kinetic energy, the fluctuating kinetic energy and the enstrophy, defined respectively as:

$$E_k(t^*) = \frac{\rho}{2} \int_{\Omega_{t^*}} \overline{\mathbf{v}} \cdot \overline{\mathbf{v}}\, d\Omega\,, \tag{27}$$

$$E_{kfl}(t^*) = \frac{\rho}{2} \int_{\Omega_{t^*}} \mathbf{v}_{rms} \cdot \mathbf{v}_{rms}\, d\Omega\,, \tag{28}$$

$$S(t^*) = \frac{1}{2} \int_{\Omega_{t^*}} \overline{\boldsymbol{\omega}} \cdot \overline{\boldsymbol{\omega}}\, d\Omega\,, \tag{29}$$

where $\overline{\boldsymbol{\omega}}$ is the vorticity computed with the phase averaged velocity, $\overline{\boldsymbol{\omega}} = \nabla \times \overline{\mathbf{v}}$. These quantities provide information on the nature of the flow and in some cases these can be measured experimentally. For example, the total kinetic energy of the blood flow in healthy and diseased left ventricles have been measured with 4D Magnetic Resonance Imaging in [2], where the results obtained from the measurement of the kinetic energy were tentatively linked to a physiological or pathological condition of the patient. This method could be used to evaluate the results of simulations on patient-specific or idealized and parametrized geometries to study particular pathologies, such as mitral valve regurgitation or atrial fibrillation. The values of the total kinetic energy in the LV and LA obtained with the VMS-LES model, the SUPG stabilization and published in [2] are reported in Table 1. We notice

that the results obtained with VMS-LES and SUPG stabilization models are very similar and that we obtain values that are two times larger with respect to the experimental results for the healthy LV. This could be due to a different choice of the measurement regions or to a higher velocity in the LV in our model due to possible geometrical variations.

The same quantities can be divided by the blood mass in the LV and LA, respectively, in order to obtain values that can be easily compared between the LA and the ventricle and among different patients. Therefore, we define

$$\rho_{Ek}(t^*) = \frac{E_k(t^*)}{\rho|\Omega(t^*)|} \qquad \rho_{Ekfl}(t^*) = \frac{E_{kfl}(t^*)}{\rho|\Omega(t^*)|} \qquad \rho_S(t^*) = \frac{S(t^*)}{\rho|\Omega(t^*)|}\,, \qquad (30)$$

and we study their trend during a complete heartbeat. In Figures (9-11) we report the specific kinetic energy, the specific fluctuating kinetic energy and the specific enstrophy versus time for the LA and the LV and compare the results obtained with VMS-LES and SUPG stabilization. First we remark that the results obtained with the two different stabilization methods are very similar and in some cases, for example for the total kinetic energy, they cannot be distinguished at all. The specific kinetic energy $\rho_{Ek}(t^*)$ shows a very large peak corresponding to the E-wave in the LA and, with a small delay, in the LV too. A peak corresponding to the A-wave is visible in the LA, while the kinetic energy of the LV does not change much during the A-wave. During systole, there is another peak in the LV when blood flows through the aorta and then the kinetic energy shows the minimum. In the LA, the refilling leads to a smoother increase of kinetic energy; we remark also that the minimum value of $\rho_{Ek}(t^*)$ in the LA is higher than the one in the LV. The fluctuating kinetic energy reported in Figure 10 shows a different trend with only one large peak after the E-wave in both the LA and LV. These peaks are delayed with respect to the kinetic energy and they correspond to the breakup of the large vortex structures created during the E-wave. This means that the breakup process is highly variable among heartbeats and we suggest that it could be indicative of transition to turbulence. We also remark that the trend of $\rho_{Ekfl}(t^*)$ in the LA is flatter than in the LV; this means that the LA flow is more regular among heartbeats. Finally, we analyze the specific enstrophy $\rho_S(t^*)$. This quantity is strongly linked to the dissipation of the kinetic energy of the flow and it is an indicator of high or low vorticity and transition to turbulence [44, 45]. In Figure 11, we report the specific enstrophy as a function of time. We notice again the presence of a peak corresponding to the E-wave with some delay in both the LA and the LV and a second stronger peak in the LA. The peaks correspond to the time instants when the kinetic energy is mostly dissipated. Moreover, we remark that the values between the LA and the LV are quite similar, so we can assume that the blood flow in the two chambers shows similar vorticity and dissipative features.

Several other indicators have been introduced to assess the cardiovascular situation of patients [6, 46]. In this work, we study the Oscillatory Shear Index (OSI) and the Relative Residence Time (RRT) which are both based on the computation of the Wall Shear Stress
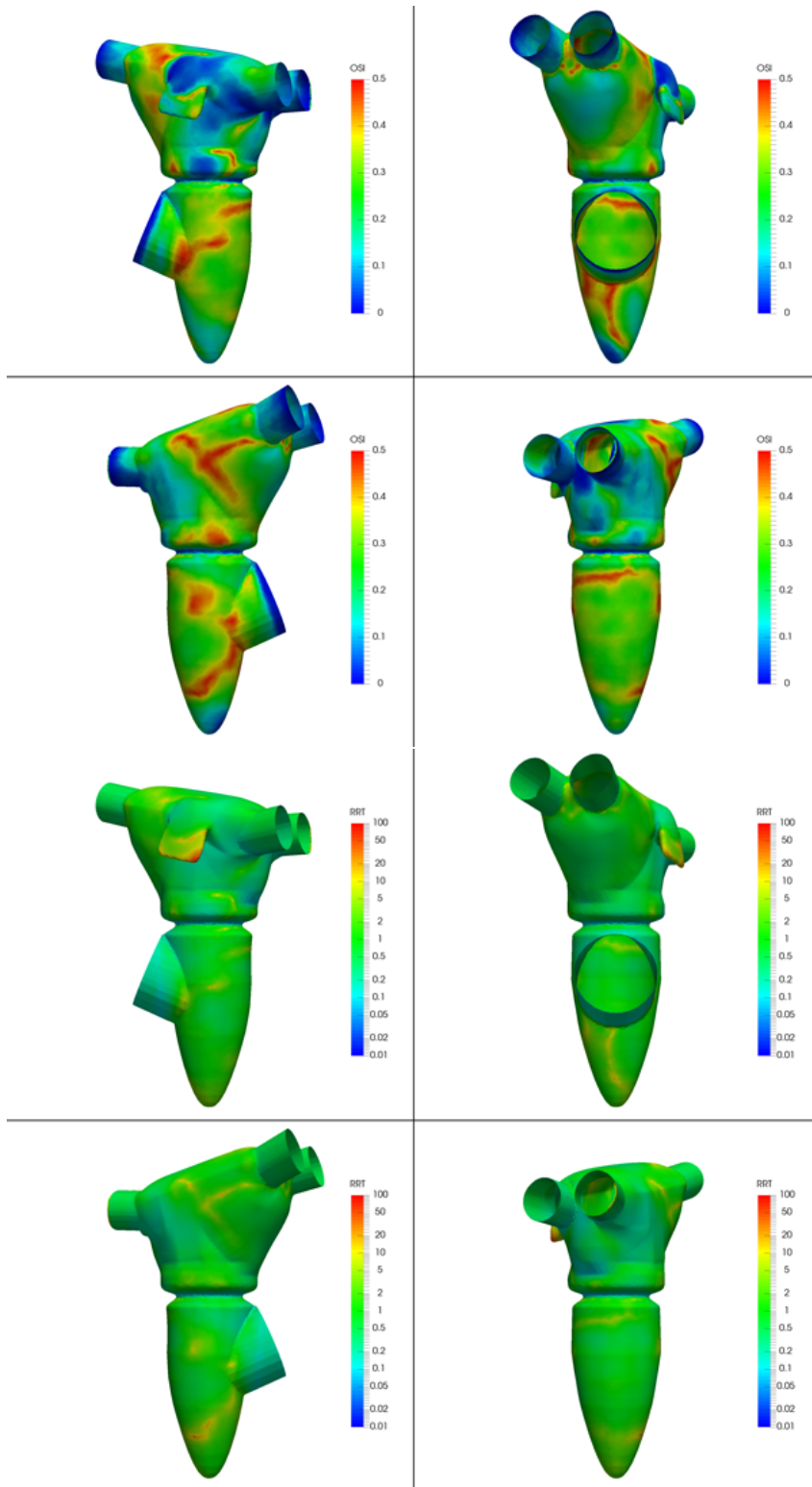
Figure 12: Oscillatory Shear Index and Relative Residence Time computed by using the phase averaged wall shear stress, VMS-LES model.

21

(WSS). These are defined, respectively, as:

$$OSI = 0.5 \left(1 - \frac{\left| \int_0^T \overline{WSS} \, dt \right|_2}{\int_0^T \left| \overline{WSS} \right|_2 dt} \right) , \qquad (31)$$

$$RRT = \left[\frac{(1 - 2\,OSI)}{T} \left| \int_0^T \overline{WSS} \, dt \right|_2 \right]^{-1} , \qquad (32)$$

where $\left| \cdot \right|_2$ denotes the Euclidean modulus of a vector. The OSI is mostly used in arteries when studying the deposition of plaques that can lead to stenosis formation or atherosclerosis. It has been suggested that the OSI can be a valuable indicator of the locations where the deposition of material is more likely to happen in arteries [6]. The RRT is an indicator of how much time a blood particle spends in the vicinity of a wall, so it can be linked to a weak blood turnover in the regions where RRT is high [46]. In Figure 12 on the left, we report the OSI as computed using the WSS based on the phase averaged velocity. The OSI is higher in the LA in the opposite wall with respect to the LAA and in the LV it is asymmetric with one side where the oscillations are higher in the top part and the other side where oscillations are higher in the LV bottom. In Figure 12 (right), the RRT is shown. This quantity shows a few spots where it is high, in the bottom of the LAA and in the LV bottom. In particular the very high values in the LAA have been already reported in simulations of patient-specific geometries [21, 23], so our model can reproduce also this characteristic feature of the flow in the LA.

4. Conclusions

In this work, we studied the hemodynamics of an idealized left heart. We developed a computational model for the left heart geometry and we prescribed the wall displacement based on physiological data. We considered the VMS-LES method to stabilize the discretized incompressible Navier-Stokes equations in the ALE reference system used to account for the moving domain. Valves are modeled by means of the resistive method, which involves a modification of the momentum equation in the fluid problem. Hence, in this paper, we accordingly modified the VMS-LES to account for the presence of the valves induced by the resistive method. The resulting system of equations has been solved through high performance computing platform and the LES quality of the results has been confirmed by means of the Pope indicator [27]. We analyzed and post-processed the numerical results to obtain clinically meaningful medical indicators and compared them with experimental and numerical results available in literature. VMS-LES and SUPG stabilization techniques produced very similar results in this setup. Our model provides an overall detailed description of the blood flow in the left heart and we suggest it can be employed in the future to perform parametric studies of specific heart pathologies, such as mitral flow regurgitation, or to study blood flow at faster heartbeat rate. In these cases, the turbulence level of the flow is larger than in the physiological case, and a VMS-LES model can correctly capture all the small structures with a smaller dissipation level than the one

introduced by SUPG. The results indicate that a transition to turbulence is more likely to occur after the E-wave, being initiated by the breakup of the large vortex structures in the LV.

Acknowledgements

References

[1] M. Carlsson, E. Heiberg, J. Töger, and H. Arheden. Quantification of left and right ventricular kinetic energy using four-dimensional intracardiac magnetic resonance imaging flow measurements. *American Journal of Physiology: Heart and Circulatory Physiology*, 302(4):893-900, 2012.

[2] M. Kanski, P. Arvidsson, J. Töger, R. Borgquist, E. Heiberg, M. Carlsson, and H. Arheden. Left ventricular fluid kinetic energy time curves in heart failure from cardiovascular magnetic resonance 4D flow data. *Journal of Cardiovascular Magnetic Resonance*, 17:111, 2015.

[3] N. Kawel-Boehm, A. Maceira, E.R. Valsangiacomo-Buechel, J. Vogel-Claussen, E.B. Turkbey, R. Williams, S. Plein, M. Tee, J. Eng, and D.A. Bluemke. Normal values for cardiovascular magnetic resonance in adults and children. *Journal of Cardiovascular Magnetic Resonance*, 17-29, 2015.

[4] S. Cimino, G. Pedrizzetti, G. Tonti, E. Canali, V. Petronilli, L. De Luca, et al.. In vivo analysis of intraventricular fluid dynamics in healthy hearts. *European Journal of Mechanics - B/Fluids*, 35:40-46, 2012.

[5] M. Markl, A.Frydrychowicz, S. Kozerke, M. Hope, and O. Wieben, 4D Flow MRI. *Journal of Magnetic Resonance Imaging*, 36(5):1015-1036, 2012.

[6] D.N. Ku, D.P. Giddens, C.K. Zarins, and S. Glagov. Pulsatile flow and athero-sclerosis in the human carotid bifurcation. Positive correlation between plaque location and low oscillating shear stress. *Arteriosclerosis*, 5:293-302, 1985.

[7] L. Formaggia, A. Quarteroni, and A. Veneziani. *Cardiovascular Mathematics: Modeling and Simulation of the Circulatory System*. Springer, 2009.

[8] A. Quarteroni, A. Manzoni, and C. Vergara. The cardiovascular system: Mathematical modelling, numerical algorithms and clinical applications. *Acta Numerica*, 26:365-590, 2017.

[9] A. Quarteroni, T. Lassila, S. Rossi, and R. Ruiz-Baier. Integrated Heart - Coupling multiscale and multiphysics models for the simulation of the cardiac function. *Computer Methods in Applied Mechanics and Engineering*, 314:345-407, 2017.

[10] S. Sugiura, T. Washio, A. Hatano, J. Okada, H. Watanabe, and T. Hisada. Multi-scale simulations of cardiac electrophysiology and mechanics using the University of Tokyo heart simulator. *Progress in Biophysics and Molecular Biology*, 110:380-389, 2012.

[11] A. Gerbi, L. Dedè and A. Quarteroni. A monolithic algorithm for the simulation of cardiac electromechanics in the human left ventricle. *MOX Report* 51/2017, Politecnico di Milano, 2017.

[12] M. Fedele, E. Faggiano, L. Dedè, and A. Quarteroni. A patient-specific aortic valve model based on moving resistive immersed implicit surfaces. *Biomechanics and Modeling in Mechanobiology*, 16(5):1779-1803, 2017.

[13] M. Nobili, U. Morbiducci, R. Ponzini, C.D. Gaudio, A. Balducci, M. Grigioni, F.M. Montevecchi, and A. Redaelli. Numerical simulation of the dynamics of a bileaflet prosthetic heart valve using a fluid-structure interaction approach. *Journal of Biomechanics*, 41:2539-2550, 2008.

[14] P. Tricerri, L. Dedè, A. Gambaruto, A. Quarteroni, and A. Sequeira. A numerical study of isotropic and anisotropic constitutive models with relevance to healthy and unhealthy cerebral arterial tissues. *International Journal of Engineering Science*, 101126-155, 2016.

[15] M.S. Sacks, W.D. Merryman, and D.E. Schmidt. On the biomechanics of heart valve function. *Journal of Biomechanics*, 42:1804-1824, 2009.

[16] MD De Tullio, A Cristallo, E Balaras, and R Verzicco. Direct numerical simulation of the pulsatile flow through an aortic bileaflet mechanical heart valve. *Journal of Fluid Mechanics*, 622:259-290, 2009.

[17] B.E. Griffith. Immersed boundary model of aortic heart valve dynamics with physiological driving and loading conditions. *International Journal for Numerical Methods in Biomedical Engineering*, 28(3):317-345, 2012.

[18] A. Tagliabue. Mathematical and Numerical Modeling of Blood Flow in an Idealized Left Ventricle. PhD Thesis, Politecnico di Milano, 2016.

[19] A. Tagliabue, L. Dedè, and A. Quarteroni, Fluid dynamics of an idealized left ventricle: the extended Nitsche's method for the treatment of heart valves as mixed time varying boundary conditions. *International Journal for Numerical Methods in Fluids*, 85(3):135-164, 2017.

[20] A. Tagliabue, L. Dedè, and A. Quarteroni. Complex blood flow patterns in an idealized left ventricle: A numerical study. *Chaos*, 27:093939, 2017

[21] A. Masci, M. Alessandrini, D. Forti, F. Menghini, L. Dedè, C. Tommasi, A. Quarteroni, and C. Corsi. A Patient-Specific Computational Fluid Dynamics Model of the Left Atrium in Atrial Fibrillation: Development and Initial Evaluation. Proceedings of the Functional Imaging and Modelling of the Heart conference, FIMH 2017, LNCS 10263, pp. 392-400, 2017.

[22] C. Chafna, S. Mendez, and F. Nicoud. Image based Large-Eddy Simulation in a realistic left heart. *Computers & Fluids*, 94:173-187, 2014.

[23] R. Koizumi, K. Funamoto, T. Hayase, Y. Kanke, M. Shibata, Y. Shiraishi, and T. Yambe. Numerical analysis of hemodynamic changes in the left atrium due to atrial fibrillation. *Journal of Biomechanics*, 48:472-478, 2015.

[24] T. Korakianitis and Y. Shi. Numerical simulation of cardiovascular dynamics with healthy and diseased heart valves. *Journal of Biomechanics*, 39:1964-1982, 2006.

[25] C.M. Colciago, S. Deparis, and A. Quarteroni. Comparisons between reduced order models and full 3D models for fluid-structure interaction problems in hemodynamics. *Journal of Computational and Applied Mathematics*, 265:120-138, 2014.

[26] A. Quarteroni, A. Manzoni, and F. Negri, *Reduced Basis Methods for Partial Differential Equations. An Introduction.* Springer, Unitext Series, Vol. 92, 2015.

[27] S.B. Pope. Ten questions concerning the large-eddy simulation of turbulent flows. *New Journal of Physics*, 6(35), 2004.

[28] M. Germano, U. Piomelli, P. Moin, and W.H. Cabot. A dynamic subgrid-scale eddy viscosity model. *Physics of Fluids*, 3(7), 1991.

[29] Y. Bazilevs, V.M. Calo, J.A. Cottrell, T.J.R. Hughes, A. Reali, and G. Scovazzi. Variational multiscale residual-based turbulence modeling for Large Eddy Simulation of incompressible flows. *Computer Methods in Applied Mechanics and Engineering*, 197:173-201, 2007.

[30] S.N. Doost, L. Zhong, B. Su, and Y.S. Morsi. The numerical analysis of non-Newtonian blood flow in human patient-specific left ventricle. *Computer Methods and Programs in Biomedicine*, 127:232-247, 2016.

[31] A.A. Johnson and T.E. Tezduyar. Mesh update strategies in parallel finite element computations of flow problems with moving boundaries and interfaces. *Computer Methods in Applied Mechanics and Engineering*, 119:73-94, 1994.

[32] D. Forti and L. Dedè. Semi-implicit BDF time discretization of the Navier-Stokes equations with VMS-LES modeling in a High Performance Computing framework. *Computers & Fluids*, 117:168-182, 2015.

[33] A.S. Patelli, L. Dedè, T. Lassila, A. Bartezzaghi, and A. Quarteroni. Isogeometric approximation of cardiac electrophysiology models on surfaces: an accuracy study with application to the human left atrium. *Computer Methods in Applied Mechanics and Engineering*, 317:248-273, 2017.

[34] F. Menghini, L. Dedè, D. Forti, and A. Quarteroni. Hemodynamics in a left atrium based on a

Variational Multiscale-LES numerical model. *MOX report* 47/2017, Politecnico di Milano, 2017.

[35] M. Korhonen, J. PArkkonen, M. Hedman et al.. Morphological features of the left atrial appendage in consecutive coronary computed tomography angiography patients with and without atrial fibrillation. *PLoS ONE*, 12(3), 2017.

[36] C. Wiggers. *Circulation in Health and Disease.* Lea & Febiger, Philadelphia, 1915.

[37] F. Domenichini, G. Pedrizzetti, and B. Baccani. Three-dimensional filling flow into a model left ventricle. *Journal of Fluid Mechanics*, 539:179-198, 2005.

[38] M.C. Hsu, D. Kamensky, Y. Bazilevs, M.S. Sacks, and T.J.R. Hughes, Fluid-structure interaction analysis of bioprosthetic heart valves: significance of arterial wall deformation. *Computational Mechanics*, 54(4):1055-1071, 2014.

[39] Y. Bazilevs, V.M. Calo, T.J.R. Hughes, and Y. Zhang. Isogeometric fluid-structure interaction: theory, algorithms and computations. *Computational Mechanics*, 43:3-37, 2008.

[40] Y. Bazilevs, J.R. Gohean, T.J.R. Hughes, R.D. Moser, and Y. Zhang. Patient-specific Isogeometric fluid-structure interaction analysis of thoracic aortic blood flow due to implantation of the Jarvik 2000 left ventricular assist device. *Computer Methods in Applied Mechanics and Engineering*, 198: 3534-3550, 2009.

[41] A. Quarteroni, A. Veneziani, and C. Vergara. Geometric multiscale modeling of the cardiovascular system, between theory and practice. *Computer Methods in Applied Mechanics and Engineering*, 302:193-252, 2016.

[42] LifeV website: <www.lifev.org>.

[43] R. Mittal, J.H. Seo, V. Vedula, Y.J. Choi, H. Liu, H.H. Huang, S. Jain et al.. Computational modeling of cardiac hemodynamics: current status and future outlook. *Journal of Computational Physics*, 305: 1065-1082, 2016.

[44] M. Umeki. Numerical simulation of plane Poiseuille turbulence. *Fluid Dynamics Research*, 13:67-79, 1994.

[45] A.R. Lupo, I.I. Mokhov, S. Dostoglou, A.R. Kunz, and J.P. Burkhardt. Assessment of the Impact of the Planetary Scale on the Decay of Blocking and the Use of Phase Diagrams and Enstrophy as a Diagnostic. *Izvestiya, Atmospheric and Oceanic Physics*, 43(1):45-51, 2007.

[46] H.A. Himburg, D.M. Grzybowski, A.L. Hazel, J.A. LaMack, X.M. Li, and M.H. Friedman. Spatial comparison between wall shear stress measures and porcine arterial endothelial permeability. *American Journal of Physiology: Heart and Circulatory Physiology*, 286: 1916-1922, 2004.

MOX Technical Reports, last issues

Dipartimento di Matematica
Politecnico di Milano, Via Bonardi 9 - 20133 Milano (Italy)

18/2018   Antonietti, P.F.; Bonaldi, F.; Mazzieri, I.
A high-order discontinuous Galerkin approach to the elasto-acoustic problem

14/2018   Cuffaro, M.; Miglio, E.; Penati, M.;Viganò, M.
Mantle upwelling driven by asymmetric sea-floor spreading at northern Mid–Atlantic ridge

15/2018   Simona, A.; Bonaventura, L.; Pugnat, T.; Dalena, B.
High order time integrators for the simulation of charged particle motion in magnetic quadrupoles

16/2018   Calissano, A.; Vantini, S.; Arnaboldi, M.
An elephant in the room: Twitter samplingmethodology.

17/2018   Agosti, A.; Giverso, C.; Faggiano, E.;Stamm,A.; Ciarletta, P.
A personalized mathematical tool for neuro-oncology: a clinical case study

13/2018   Gandelli, E.; Penati, M.;Quaglini, V.;Lomiento, G.; Miglio, E.; Benzoni, G.M.
A novel OpenSees element for single curved surface sliding isolators

12/2018   Dal Santo, N.; Deparis, S.; Manzoni, A.; Quarteroni, A.
Multi space reduced basis preconditioners for large-scale parametrized PDEs

11/2018   Delpopolo Carciopolo L.; Bonaventura L.; Scotti A.; Formaggia L.
A conservative implicit multirate method for hyperbolic problems

10/2018   Menafoglio, A.; Gaetani, G.; Secchi, P.
Random Domain Decompositions for object-oriented Kriging over complex domains

09/2018   Menafoglio, A.; Grasso, M.; Secchi, P.; Colosimo, B.M.
Profile Monitoring of Probability Density Functions via Simplicial Functional PCA with application to Image Data